ANS MC2015 - Joint International Conference Mathematics and Computation (M&C), Super Computing in Nuclear Applications (SNA) and the Monte Carlo (MC) Method • Nashville, TN • April 19-23, 2015, on CD-ROM, American Nuclear Society, LaGrange Park, IL (2015)

A HIGH-ORDER LOW-ORDER ALGORITHM WITH EXPONENTIALLY-CONVERGENT MONTE CARLO FOR THERMAL RADIATIVE TRANSFER

Simon R. Bolding* **and Jim E. Morel**
Department of Nuclear Engineering
Texas A&M University
College Station, TX 77843
sbolding@tamu.edu; morel@tamu.edu

Mathew A. Cleveland
Los Alamos National Laboratory
Los Alamos, NM 87545
cleveland@lanl.gov

ABSTRACT

We have implemented a new high-order low-order (HOLO) algorithm for solving thermal radiative transfer problems. The low-order (LO) system is based on spatial and angular moments of the transport equation and a linear-discontinuous finite-element spatial representation, producing equations similar to the standard S_2 equations. The LO solver is fully implicit in time and efficiently resolves the non-linear temperature dependence at each time step. The HO solver utilizes exponentially-convergent Monte Carlo (ECMC) to give a globally accurate solution for the angular intensity to a fixed-source, pure absorber transport problem. This global solution is used to compute consistency terms that require the HO and LO solutions to converge towards the same solution. The use of ECMC allows for the efficient reduction of statistical noise in the MC solution, reducing inaccuracies introduced through the LO consistency terms. We compare results with an implicit Monte Carlo (IMC) code for one-dimensional, gray test problems and demonstrate the efficiency of ECMC over standard Monte Carlo in this algorithm.

Key Words: hybrid Monte Carlo, residual Monte Carlo, thermal radiative transfer

I. INTRODUCTION

We have implemented a high-order low-order (HOLO) algorithm for the case of 1D gray thermal radiative transfer (TRT) problems. The governing equations are the radiation and material energy balance equations, i.e.,

$$\frac{1}{c}\frac{\partial I}{\partial t} + \mu\frac{\partial I}{\partial x} + \sigma_t I = \frac{\sigma_s}{2}\phi + \frac{1}{2}\sigma_a acT^4 \tag{1}$$

$$\rho c_v \frac{\partial T}{\partial t} = \sigma_a \phi - \sigma_a acT^4. \tag{2}$$

In the above equations x is the position, t is the time, μ is the x-direction cosine of the angular intensity $I(x,\mu,t)$, and a, c, ρ, and c_v are the radiation constant, speed of light, mass density, and specific heat; σ_a, σ_s, and σ_t are the absorption, scattering, and total cross sections (cm^{-1}), respectively. The desired unknowns are the material temperature $T(x,t)$ and the scalar radiation intensity $\phi(x,t) = \int_{-1}^{1} I(x,\mu,t)\mathrm{d}\mu$. The scalar intensity is related to the radiation energy density as $E = \phi/c$. The equations are strongly coupled through the gray Planckian emission source $\sigma_a acT^4$, which is a nonlinear function of temperature, and the absorption term $\sigma_a\phi$. In general, the material properties are a function of

*LA-UR-14-29653

T. The temperature dependent material properties and absorption- reemission physics lead to systems that require solution in a mix of streaming and optically-thick, diffusive regions.

Monte Carlo (MC) solution to the TRT equations is typically achieved by the implicit Monte Carlo (IMC) method [**?**]. This method linearizes Eq. (1) & Eq. (2) over a discrete time step. The linearization of the system produces a transport equation that contains an approximate emission source and an effective scattering cross section representing absorption and reemission of photons over a time step. This transport equation is solved using MC. The MC simulation tallies energy absorption over a discretized spatial mesh. The energy absorption in each mesh cell is used to directly estimate a new end of time step temperature in that cell. In optically thick regions, or for large time steps, the effective scattering dominates interactions. In these diffusive regions IMC becomes computationally expensive. Acceleration methods typically attempt to improve efficiency by allowing particles to take discrete steps through optically thick regions based on a discretized diffusion approximation [**?**,**?**]. In IMC the approximate linearization of the emission source is not iterated on within a time step due to the large computational cost of the MC transport each time step; this imposes a limit on the time step size to produce physically accurate results [**?**].

Moment-based hybrid Monte Carlo (MC) methods provide an alternative solution method. Recent work has focused on so-called high-order low-order (HOLO) approaches [**?**,**?**,**?**,**?**]. Such methods utilize a low-order (LO) operator based on angular moments of the transport equation, formulated over a fixed spatial mesh. Physics operators that are time consuming for MC to resolve, e.g., absorption-reemission and scattering events, are moved to the LO system. Newton methods allow for non-linearities in the LO equations to be fully resolved efficiently [**?**]. The high-order (HO) transport equation is defined by Eq. (1), with sources that are truly implicit in time estimated from the LO solution. The HO equation is solved via MC to produce a high-fidelity solution for the angular intensity. The MC estimate of the angular intensity is used to estimate consistency terms, present in the LO equations, that require the LO system to preserve the angular accuracy of the MC solution. The HO system does not directly estimate a new material temperature, eliminating stability issues that require linearization of the emission source.

Sufficient MC histories must be performed to eliminate statistical noise in the consistency terms that can contaminate the LO solution. Exponentially-convergent Monte Carlo (ECMC)[**?**] provides an algorithm that can efficiently reduce statistical noise to the same order as the HOLO iteration error with significantly less particle histories than standard MC. In particular, ECMC is exceptionally efficient in time-dependent TRT problems because information about the intensity from the previous time step can be used as an accurate initial guess for the end of time step intensity. Additionally, no particle histories are required in regions of the problem where the problem is in equilibrium, similar to [**?**]. However, implementation of ECMC is non-trivial, requiring a finite-element representation of the solution in all phase-space variables. The fundamental transport of particles is the same as standard Monte Carlo transport codes, but the source will now contain positive and negative weight particles.

Our ECMC solver contains similarities to the residual Monte Carlo (RMC) HO solver in [**?**], with some key differences. The RMC algorithm uses a particular, fixed estimate of the solution to significantly reduce the statistical noise in the simulation compared to a standard MC simulation. The guess for the solution is chosen to produce only sources on the faces of cells, reducing the dimension of the phase-space to be sampled [**?**]. The RMC algorithm uses a piecewise constant trial space representation for the intensity in x and μ. The primary difference between the methods is that ECMC iteratively estimates the solution, in batches, producing a known MC estimate of the error in that estimate. The ECMC algorithm also uses a linear-discontinuous finite-element (LDFE) trial space to represent the intensity, although the RMC algorithm could similarly be formulated with an LDFE representation. The LDFE representation introduces significant implementation complexity. The formulation of the residual in [**?**] can produce

minimal statistical noise in slowly varying problems where the behavior of the system is near equilibrium. The ECMC algorithm has similar statistical efficiency by choosing the old intensity as the initial guess to the algorithm. The ECMC algorithm will generally be more efficient in cases where the solution varies greatly over a time step or when very low statistical noise is desired. Generally, the minimum number of histories per batch to obtain convergence with the LDFE trial space is larger than a piece-wise constant representation because additional histories are needed to sufficiently estimate the first moment in x and μ of the intensity. It is noted that our formulation of the LO equations is in great contrast to the formulation in [**?**].

In this work, we demonstrate the utility of an S_2-like LO operator [**?**] in conjunction with an ECMC method [**?**] for the HO solver. The ECMC algorithm uses information about the intensity from the previous time step to reduce statistical noise to the same order as the HOLO iteration error with significantly less particle histories than standard MC simulations, with less computational cost than IMC per history. We have derived the LO operator directly from the transport equation, using a linear-discontinuous (LD) finite-element (FE) spatial discretization, such that the HO and LO solutions are converging towards the same solution. Herein we describe the algorithm and present results for two??? test problems.

II. Overview of the HOLO Algorithm

For simplicity, our HOLO method will use a backwards Euler discretization in time, as well as constant specific heats and cell-wise constant opacities. The time discretized equations are

$$\mu\frac{\partial I^{n+1}}{\partial x}+\left(\sigma_t+\frac{1}{c\Delta t}\right)I^{n+1}=\frac{\sigma_s}{2}\phi^{n+1}+\frac{1}{2}\left(\sigma_a acT^4\right)^{n+1}+\frac{I^n}{c\Delta t} \tag{3}$$

$$\rho c_v\frac{T^{n+1}-T^n}{\Delta t}=\sigma_a\phi^{n+1}-\sigma_a ac(T^4)^{n+1}. \tag{4}$$

where Δt is the time step size and the superscript n is used to indicate the n-th time step. It is noted that in IMC the time derivative in Eq. (1) is typically treated using continuous time-dependent MC over each time step. Our HO transport equation is discrete in time for easy application of ECMC and to avoid difficulties in coupling to the fully-discrete LO solver, but this does introduce some artificial propagation of energy due to the implicit time differencing, in optically thin regions.

In the HOLO context, the LO solver models the physical scattering and resolves the material temperature spatial distribution $T(x)$ at each time step. The LO equations are formed via half-range angular and spatial moments of Eq. (3) and Eq. (4), formed over a spatial finite element mesh. The angular treatment in the LO equations has the same form as those used in the hybrid-S_2 method in [**?**], with element-averaged consistency parameters that are analogous to a variable Eddington factor. If the angular consistency parameters were estimated exactly, then the LO equations are exact with respect to the chosen spatial discretization. These consistency parameters are lagged in each LO solve, estimated from the previous HO solution for $I^{n+1}(x,\mu)$, as explained below. For the initial LO solve for each time step, the parameters are calculated based on the $I^n(x,\mu)$. The LO equations always conserve total energy, independent of the accuracy of the consistency terms.

The solution to the LO system is used to construct a spatially LDFE representation of the scattering and emission sources on the right hand side of Eq. (3). This defines a fixed-source, pure absorber transport problem for the HO operator. This HO transport problem represents a characteristic method that uses MC to invert the continuous streaming plus removal operator with an LDFE representation of sources. We will solve this transport problem using ECMC. The output from ECMC is $\tilde{I}(x,\mu)$, a space-angle LDFE projection of the exact solution for $I(x,\mu)$. Once computed, $\tilde{I}(x,\mu)$ is used to directly evaluate the necessary consistency parameters for the next LO solve. Since there is a global, functional representation

of the angular intensity, LO parameters are estimated using quadrature and do not require additional tallies. The HO solution is not used to directly estimate a new temperature at the end of the time step; it is only used to estimate the spatial and angular parameters in the LO solution, which eliminates typical operator splitting stability issues that require linearization of the emission source.

The process of performing subsequential HO and LO solves, within a single time step, can be repeated to obtain an increasingly accurate solution for $\phi^{n+1}(x)$ and $T^{n+1}(x)$. Thus, the HOLO algorithm, for the n-th time step, is

1. Perform a LO solve to produce an initial guess for $T^{n+1,0}(x)$ and $\phi^{n+1,0}(x)$, based on consistency terms estimated with $\tilde{I}^n$.
2. Solve the HO system for $\tilde{I}^{n+1,k+1/2}(x,\mu)$ using ECMC, based on the current LO estimate of the emission and scattering sources.
3. Compute LO consistency parameters with $\tilde{I}^{n+1,k+1/2}$.
4. Solve the LO system using HO consistency parameters to produce a new estimate of $\phi^{n+1,k+1}$ and $T^{n+1,k+1}$.
5. Repeat 2 – 4 until convergence is achieved.
6. Store $\tilde{I}^n \leftarrow \tilde{I}^{n+1}$, and move to the next time step.

where the superscript k denotes an outer HOLO iteration. The consistency terms force the HO and LO solutions for $\phi^{n+1}(x)$ to be consistent to the order of the current HOLO iteration error.

III. Forming the Low-Order System

To form the LO system of equations, spatial moments are taken over each spatial cell i: $x \in [x_{i-1/2}, x_{i+1/2}]$, weighted with the standard linear FE interpolatory basis functions. For example, the L moment operator is defined by

$$\langle\cdot\rangle_{L,i} = \frac{2}{h_i}\int_{x_{i-1/2}}^{x_{i+1/2}} b_{L,i}(x)(\cdot)\mathrm{d}x, \tag{5}$$

where $h_i = x_{i+1/2} - x_{i-1/2}$ is the width of the spatial element and $b_{L,i}(x) = (x_{i+1/2} - x)/h_i$ is the FE basis function, for cell i, corresponding to position $x_{i-1/2}$. The right moment $\langle\cdot\rangle_R$ is defined with weight function $b_{R,i}(x) = (x - x_{i-1/2})/h_i$. Here, it is noted in this notation $\langle\phi\rangle_{L,i}$ and $\langle\phi\rangle_{R,i}$ represent spatial moments of the intensity over cell i, rather than $\phi_{L,i}$ and $\phi_{R,i}$ which represent the interior value of the linear $\phi(x)$ at $x_{i-1/2}$ and $x_{i+1/2}$. To reduce the angular dimensionality, positive and negative half-range integrals of the angular intensity are taken. The half-range averages of I are defined as $\phi^+(x) = \int_0^1 I(x,\mu)\mathrm{d}\mu$ and $\phi^-(x) = \int_{-1}^0 I(x,\mu)\mathrm{d}\mu$, respectively. Thus, in terms of half-range quantities, $\phi(x) = \phi^-(x) + \phi^+(x)$.

III.A. Radiation Energy Equations

Pairwise application of the L and R basis moments with the $+$ and $-$ half-range integrals to Eq. (3) ultimately yields four radiation moment equations per cell. As in [**?**], algebraic manipulation is performed to form intensity-weighted averages of μ, which we denote consistency terms. As an example, the final

equation resulting from application of the L moment and positive half-range integral is

$$-2\mu_{i-1/2}^{n+1,+}\phi_{i-1/2}^{n+1,+}+\{\mu\}_{L,i}^{n+1,+}\langle\phi\rangle_{L,i}^{n+1,+}+\{\mu\}_{R,i}^{n+1,+}\langle\phi\rangle_{R,i}^{n+1,+}+\left(\sigma_t^{n+1}+\frac{1}{c\Delta t}\right)h_i\langle\phi\rangle_{L,i}^{n+1,+}$$
$$-\frac{\sigma_s h_i}{2}\left(\langle\phi\rangle_{L,i}^{n+1,+}+\langle\phi\rangle_{L,i}^{n+1,-}\right)=\frac{h_i}{2}\langle\sigma_a^{n+1}acT^{n+1,4}\rangle_{L,i}+\frac{h_i}{c\Delta t}\langle\phi\rangle_{L,i}^{n,+},\quad(6)$$

where the $\phi_{i-1/2}^{+}$ and $\mu_{i-1/2}^{+}$ terms represent face-averaged quantities at $x_{i-1/2}$. The negative direction and R moment equations are derived analogously. Opacities are assumed constant over each element, evaluated at the average temperature in the element, i.e., $\sigma_a=\sigma_a([T_{L,i}+T_{R,i}]/2)$, $x\in(x_{i-1/2},x_{i+1/2})$. The element-averaged angular consistency terms are defined in terms of half-range integrals, e.g.,

$$\{\mu\}_{L,i}^{n+1,+}\equiv\frac{\langle\mu I^{n+1}\rangle_{L,i}^{+}}{\langle I^{n+1}\rangle_{L,i}^{+}}=\frac{\frac{2}{h_i}\int_0^1\int_{x_{i-1/2}}^{x_{i+1/2}}\mu\, b_{L,i}(x)I^{n+1}(x,\mu)\mathrm{d}x\mathrm{d}\mu}{\frac{2}{h_i}\int_0^1\int_{x_{i-1/2}}^{x_{i+1/2}}b_{L,i}(x)I^{n+1}(x,\mu)\mathrm{d}x\mathrm{d}\mu}.\quad(7)$$

The $\mu_{i-1/2}^{n+1,+}$ term is defined analogously and represents an angular average on the face at $x_{i-1/2}$.

III.B. Material Energy Equations

To derive the LO material energy equations, $T(x)$ is represented spatially in the LDFE trial space, i.e., $T(x)\simeq T_{L,i}b_{L,i}(x)+T_{R,i}b_{R,i}(x),\quad x\in(x_{i-1/2},x_{i+1/2})$. Similarly, the emission term is represented in the material and radiation equations with the LDFE interpolant of $T^4(x)$. The L and R spatial moments are taken of the material energy equation, using these definitions for $T(x)$ and $\sigma_a acT^4(x)$ to simplify moments. For example, the final LO material energy equation resulting from application of the L moment is

$$\frac{\rho_i c_{v,i}}{\Delta t}\left[\left(\frac{2}{3}T_{L,i}+\frac{1}{3}T_{R,i}\right)^{n+1}-\left(\frac{2}{3}T_{L,i}+\frac{1}{3}T_{R,i}\right)^{n}\right]+\sigma_a^{n+1}\left(\langle\phi\rangle_{L,i}^{+}+\langle\phi\rangle_{L,i}^{-}\right)^{n+1}$$
$$=\sigma_a^{n+1}ac\left(\frac{2}{3}T_{L,i}^4+\frac{1}{3}T_{R,i}^4\right)^{n+1}.\quad(8)$$

Because the material energy balance only contains angularly integrated quantities, there is no need to take angular moments of the above equation.

III.C. Closing the System with Information from the HO solution

The six degrees of freedom (DOF) over each cell i are the four moments $\langle\phi\rangle_{L,i}^{+}$, $\langle\phi\rangle_{R,i}^{+}$, $\langle\phi\rangle_{L,i}^{-}$, and $\langle\phi\rangle_{R,i}^{-}$ and the two spatial edge values $T_{L,i}$ and $T_{R,i}$. The four radiation and two material energy equations define a system of equations for the six DOF, coupled to other cells via upwinding in the streaming term. The relation between the volume and face averaged quantities and the angular consistency parameters (e.g., Eq. (7)) are not known a priori. A lagged estimate of I^{n+1} from the previous HO solve is used to estimate the angular consistency parameters. In the HOLO algorithm, the equations for LO unknowns at iteration $k+1$ use consistency parameters computed (via relations, e.g., Eq. (7)) using the latest HO solution $\tilde{I}^{n+1,k+1/2}$ as an approximation for $I^{n+1}(x,\mu)$. To close the LO system spatially, the usual upwinding approximation is used. For example, for positive flow (e.g., Eq. (6)) the face terms $\mu_{i-1/2}$ and $\phi_{i-1/2}$ are upwinded from the previous cell $i-1$ or from a boundary condition; the terms at $x_{i+1/2}$ are linearly

extrapolated, computed using the L and R basis moments, e.g., $\phi^+_{i+1/2} = 2\langle\phi\rangle^+_R - \langle\phi\rangle^+_L$. The HO ECMC solver computes an LDFE representation of the intensity, so the same spatial closure is used to relate volume and face averaged consistency terms. Thus, the spatial closure between the LO and HO solvers are inherently consistent. Because there are no spatial temperature derivatives, there is no need for an additional closure in T.

The LD closure is not strictly positive. In particular, for optically thick cells with a steep intensity gradient, the solution becomes negative. These negativities can also result in adjacent cells in the direction of flow. In thick regions of TRT problems, reasonably fine spatial cells can still be on the order of millions of mean free paths; negativities with a LD representation are unavoidable in practice for such cells and mesh refinement is of minimal use. Typically, for a standard LDFE method, the equations are lumped to produce a strictly positive solution for 1D [**?**]. However, standard FE lumping procedures would introduce difficulties in computing the consistency terms from the HO solution. Thus, an alternative spatial closure is used that is equivalent to the standard FE lumping procedure. The L and R moments are defined the same as before, preserving the same average within a cell, but the relation between the moments and the outflow is modified. For example, for positive μ, the outflow is now defined as $\phi^+_{i+1/2} = \langle\phi\rangle^+_R$. Because the basis function $b_{R,i}(x)$ is strictly positive, the outflow is positive. This closure is only used in cells in which negativities occur.

III.D. Solving the Non-Linear LO System

We have used Newton's method to solve the global system of coupled LO equations, based on a typical linearization of the Planckian source with opacities evaluated at lagged temperatures, as described in [**?**]. Newton iterations are repeated until $\phi^{n+1}(x)$ and $T^{n+1}(x)$ are converged to a desired relative tolerance. The lumping-equivalent discretization discussed above is used for cells where the solution for ϕ^{n+1} becomes negative. When negativities are detected, the lumping-equivalent discretization is used within those cells and that Newton step is repeated.

IV. The ECMC High Order Solver

The transport equation to be solved by the HO solver is

$$\mu\frac{\partial I^{n+1,k+1/2}}{\partial x} + \left(\sigma_t^k + \frac{1}{c\Delta t}\right) I^{n+1,k+1/2} = \frac{\sigma_s}{2}\phi^{n+1,k} + \frac{1}{2}\left(\sigma_a^k acT^4\right)^{n+1,k} + \frac{\tilde{I}^n}{c\Delta t} \tag{9}$$

where the superscript k represents the outer HOLO iteration index. Material property indices will be suppressed from now on. Here, $k + 1/2$ denotes the ECMC solution within outer HOLO iteration k, whereas k and $k + 1$ represent successive LO solves. The sources at k in Eq. (9) are estimated by the previous LO solution. Cross sections are evaluated at $T^{n+1,k}$. As all sources on the right side of the equation are known, this defines a fixed-source, pure absorber transport problem. We will solve this equation using ECMC. A more detailed description of the ECMC method can be found in [**?**], but a brief overview is given here.

In operator notation, the previous equation can be written as

$$\mathbf{L}^k I^{n+1,k+1/2} = q^k \tag{10}$$

where $I^{n+1,k+1/2}$ is the transport solution of the angular intensity based on the k-th LO estimate of q^k. The linear operator $\mathbf{L}^k$ is the streaming plus removal operator defined by the left hand side of Eq. (3). The m-th approximate LDFE solution to Eq. (10) (m is the index of inner HO batches) is represented as $\tilde{I}^{n+1,(m)}$.

The m-th residual is defined as $r^{(m)} = q - \mathbf{L}\tilde{I}^{n+1,(m)}$. For reference, the residual at iteration m in the HO solve is

$$r^{(m),k+1/2} = \frac{\sigma_s}{2}\phi^{n+1,k} + \frac{1}{2}\left(\sigma_a acT^4\right)^{n+1,k} + \frac{\tilde{I}^n}{c\Delta t} - \left(\mu\frac{\partial \tilde{I}^{n+1,k+1/2}}{\partial x} + \left(\sigma_t + \frac{1}{c\Delta t}\right)\tilde{I}^{n+1,k+1/2}\right)^{(m)} \tag{11}$$

where the k terms are LD in space on the coarsest mesh and are not recalculated at any point during the HO solve. The functional form of $\tilde{I}^n$ is defined from the final HO solution of the previous time step.

To define the ECMC algorithm, the HOLO iteration indices are dropped, as the LO estimated q^k and $\mathbf{L}^k$ remain constant over the entire HO solve. Addition of $\mathbf{L}I^{n+1} - q = 0$ to the residual equation and manipulation of the result yields the error equation

$$\mathbf{L}(I^{n+1} - \tilde{I}^{n+1,(m)}) = \mathbf{L}\epsilon^{(m)} = r^{(m)} \tag{12}$$

where I^{n+1} is the exact solution and $\epsilon^{(m)}$ is the error in $\tilde{I}^{n+1,(m)}$. The $\mathbf{L}$ operator in the above equation is inverted yielding the Monte Carlo LDFE projection of the error in $\tilde{I}^{n+1,(m)}$, i.e.,

$$\tilde{\epsilon}^{(m)} = \mathbf{L}^{-1}r^{(m)} \tag{13}$$

where $\mathbf{L}^{-1}$ is the Monte Carlo inversion of the streaming and removal operator. This inversion is strictly a standard Monte Carlo simulation. The space-angle moments of the error computed in $\tilde{\epsilon}^{(m)}$ are added to the moments of $\tilde{I}^{n+1}, (m)$ to produce a more accurate solution.

Here, we emphasize the solution $\tilde{I}^{n+1,(m)}$ represents the projection of the exact Monte Carlo solution onto the trial space. This is in general far more accurate than a standard finite element solution. For example, in typical IMC calculations the average energy deposition within a cell is computed using a standard path-length volumetric flux tally; the zeroth moment of the LDFE projection of $\tilde{\epsilon}$ is computed using an equivalent tally. The primary truncation error is in the LD representation of the right hand side source terms. Volumetric flux tallies over each space-angle element are required to represent $\tilde{\epsilon}^{(m)}$. The tallies are given in Appendix???

The ECMC algorithm is

1. Initialize the guess for $\tilde{I}^{n+1,(0)}$ to $\tilde{I}^n$ or the projection of $\tilde{I}^{n+1}$ from the latest HO solve
2. Compute $r^{(m)}$.
3. Perform a MC simulation to obtain $\tilde{\epsilon}^{(m)} = \mathbf{L}^{-1}r^{(m)}$
4. Compute a new estimate of the intensity $\tilde{I}^{n+1,(m+1)} = \tilde{I}^{n+1,(m)} + \tilde{\epsilon}^{(m)}$
5. Repeat steps 2 – 4 until desired convergence criteria is achieved.

The initial guess for the angular intensity $I^{n+1,(0)}$ is computed based on the previous solution for $\tilde{I}^n$. This is a critical step in the algorithm; it significantly reduces the required number of particles per time step because the intensity does not change drastically between time steps in optically thick regions. It is noted that the ECMC batch (steps 1-4 of the algorithm) results in essentially the same estimate of the solution as the residual formulation used in [**?**]. The primary difference is that our method uses an LDFE trial space, and we are able to use our new estimate of the solution to recompute a residual.

Exponential convergence is obtained because with each batch a better estimate of the solution is being used to compute the new residual, decreasing the magnitude of the Monte Carlo source each iteration m, relative to the solution I^{n+1}. Each Monte Carlo estimate of the moments of ϵ still has a statistical uncertainty that

is governed by the standard $1/\sqrt{N}$ convergence rate [**?**]. If the statistical estimate of $\tilde{\epsilon}$ is not sufficiently accurate, then the iterations would diverge. It is noted that although the variance in tallies of $\epsilon^{(m)}$ can be estimated with the sample variance of histories, the variance in the moments of $I^{n+1,(m)}$ cannot be easily estimated due to the correlation between $I^{n+1,(m)}$ and the source $r^{(m)}$.

Because the exact angular intensity does not in general lie within the LDFE trial space, the iterative estimate of the error will eventually stagnate once the error cannot be sufficiently represented by a given FE mesh. Although mesh refinement is not performed in the calculations presented here, an adaptive $h-$refinement algorithm has been implemented that can be used to allow the system to continue converging towards the exact solution [**?**,**?**]. In general, for TRT problems, optically thick and slowly varying regions of the problem do not require as refined of a mesh to accurately capture the solution because there is less variation in the angular dependence of the solution. Once error stagnation has occurred, additional histories can be performed with a fixed residual source to estimate the remaining error in the current solution. Although the remaining error will converge statistically at a standard $1/\sqrt{N}$ convergence rate, the remaining error will be much smaller than a standard MC simulation, producing a much more efficient solution method overall.

IV.A. Variance Reduction and Source Sampling

As in [**?**], because we are solving a pure absorber problem with Monte Carlo, we will allow particles to stream without absorption to reduce statistical variance in the tallies. The weight of particles is reduced deterministically along the path as they stream, with no need to sample a path length. Because particles are exponentially attenuated, the normalized weight is adjusted as $w(x,\mu) = w(x_0,\mu)\exp(-\sigma|(x-x_0)/\mu|)$, where x_0 is the starting location of the path. The tallies account for the continuously changing weight, as given in Appendix???. Histories are allowed to stream in this manner for 6 mean free paths before switching to analog path length sampling; this limits the tracking of very small weight histories. The choice of 6 mean free paths allows particles to continuously deposit weight until they reach 0.25% of their original weight.

As another way to improve efficiency, a modified systematic sampling method [**?**] was used for determining source particle locations. The goal is to effectively distribute particle histories to regions of importance, but to sample a sufficient number of histories in less probable regions to prevent large statistical noise. However, there is no need to sample histories in regions in equilibrium. The residual gives a good indication of where histories are most likely to contribute to the error, particularly in optically thick cells where particles do not transport long distances. The residual consists of both face and volumetric sources [**?**]. In the sampling algorithm the number of particle histories sampled in each space-angle cell is predetermined and proportional to the magnitude of the residual, including face and volumetric sources, within that cell. Then, for the predetermined number of histories within a cell, the source location is randomly sampled according to the residual source distribution of that cell. There is a relative probability cutoff such that cells with an insignificant residual will have no histories sampled there. In these regions the problem is remaining in equilibrium and the solution is known exactly. For cells that are significant, but have a predetermined number of histories below some preset minimum N_{min}, the number of histories sampled in that cell is set to N_{min}. This is to limit bad statistics in low probability cells (this would be important for adaptively refined meshes). In the simulations performed for this work $N_{min} = 1$. This choice was made for comparing to IMC to keep the total number of histories per time step constant throughout the entire simulation. The relative probability cutoff was 10^{-5}.

For the HO solver, in cells near the radiation wave front, the LDFE trial space can result in negativities in $\tilde{I}^{n+1}(x,\mu)$, similar to the LO solver. We currently force the solution within negative cells to be positive, after each batch. The methodology for enforcing positivity is given in Appendix???. Although the modified

solution is physical, it will not satisfy the residual equation very accurately. Thus, error stagnation will rapidly occur. At the end of the HO solve, the strictly positive solution can be used to compute consistency terms.

V. Results

We will compare results of the HOLO method to IMC with a source tilting algorithm [**?**]. In IMC the material and radiation energy fields are discretized spatially to solve for cell-averaged values. Inaccurate spatial representation of the emission source over a cell can result in energy propagating through the domain artificially fast, yielding non-physical results referred to as "teleportation error" [**?**]. The IMC method uses a fixup known as source tilting to mitigate this problem. Source tilting reconstructs a more accurate linear-discontinuous representation of the emission source within a cell based on the cell-averaged material temperatures in adjacent cells. This reconstruction is not necessary in our method because of the LDFE representation of the emission source. We will also demonstrate the efficiency advantage of ECMC in our HOLO algorithm by comparing the results to the same HOLO algorithm if the HO solver is replaced with a standard Monte Carlo (SMC) simulation.

V.A. Marshak Wave

For the first problem, the radiation and material energies are initially in equilibrium at 2.5×10^{-5} keV. An isotropic incident intensity of 0.150 keV is applied at $x = 0$; the incident intensity on the right boundary is 2.5×10^{-5} keV. The material properties are $\rho = 1$ g cm^{-3} and $c_v = 0.013784$ jks/keV-g. The absorption cross section varies as $\sigma(T) = 0.001\ \rho\ T^{-3}$ (cm^{-1}). The simulation was ran for 5 sh (1 sh = 10^{-8} s) with a fixed time step size of 0.001 sh. For comparison purposes, we have not used adaptive mesh refinement, only performed one HOLO iteration per time step, and use a fixed 3 HO batches with equal number of histories per batch. A relative tolerance of 1.E-06 in the norm of $\phi(x)$ and $T(x)$ was used for the LO newton solver. Radiation energy distributions are plotted as an equivalent temperature given by $T_r = (\phi/(ac))^{0.25}$. Cell-averaged quantities are plotted. Although scattering physics can be handled by the LO solver in this method [**?**], we have only considered problems with $\sigma_s = 0$ here.

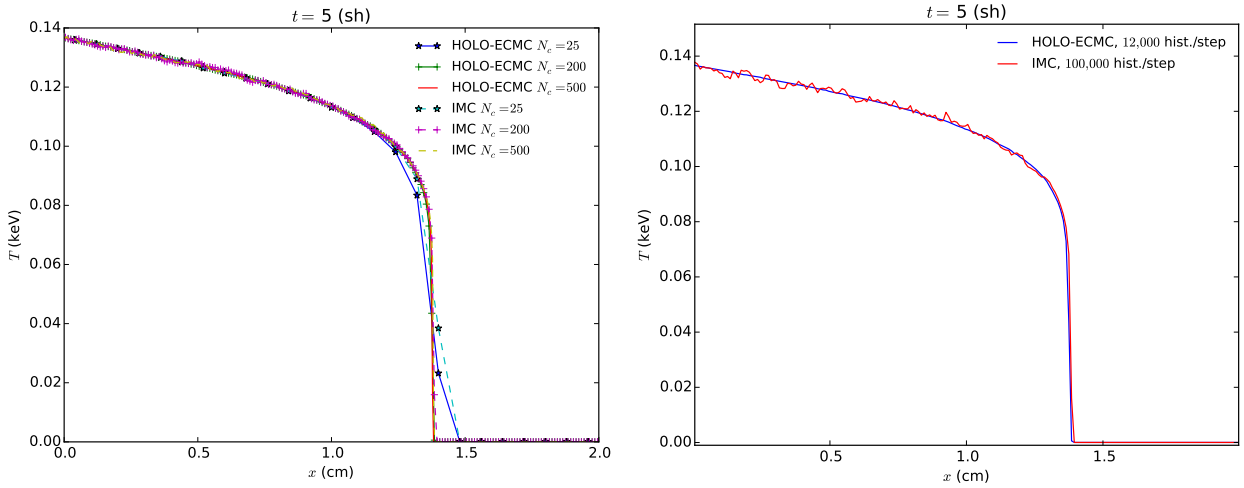

(a) Convergence of IMC and HOLO-ECMC solutions.

(b) Comparison of solutions for 200 spatial cells.

Figure 1: Comparison of solutions for Marshak wave problem at t = 5 sh.

Fig. 1a compares the cell-averaged radiation temperatures for the IMC and HOLO method with ECMC, for various number of spatial mesh cells N_c. For the HOLO solver, we have used 4 equal-sized cells in μ for

the finite-element angular mesh used by the ECMC solver. For the cases of $N_c = 25$ and $N_c = 200$, 4,000 histories per batch (12,000 per time step) were used. For $N_c = 500$, 16,000 histories per batch were used due to increased number of cells that need to be sampled. For all IMC calculations, 10^5 histories per time step were used. The solutions agree as the mesh is converged. There is similar agreement in the location of the wave front due to the linear shape of the emission source over a cell. The cells at the wave front required use of the lumping-equivalent discretization during the LO solve, resulting in strictly positive solutions.

Fig. 1b compares solutions for the case of 200 cells. For the IMC solution 10^5 histories per time step were simulated; for the HOLO method only $4,000$ histories per batch (12,000 per time step) were simulated. There is significant statistical noise in the IMC solution compared to the HOLO solution. The HOLO solution visually demonstrates no statistical noise. Since the transport solve is only determining the change over the time step, the statistical noise in the result is small relative to the magnitude of I^{n+1}. Also, the source sampling only places particles in cells where the residual is large. No particles are sampled in the equilibrium region out front of the wave.

To get a quantitative measure of the statistical accuracy of different solution methods, a spatially integrated standard deviation of independent simulations was computed. Twenty simulations for each method and problem were performed with different random number seeds. The variance of a particular cell average is computed as

$$s_i^2 = \frac{20}{20-1} \sum_{n=1}^{20} \left(\overline{\phi_i} - \phi_i^n \right)^2 \tag{14}$$

where ϕ_i^n is the cell-averaged scalar intensity for cell i from the n-th of 20 independent simulations and $\overline{\phi_i}$ is the corresponding sample mean from all simulations. To provide a normalized, spatially integrated result we compute a norm over all cells as

$$\|s\| = \sqrt{\frac{\sum_i^{N_c} s_i^2}{\sum_i^{N_c} \overline{\phi_i}^2}} \tag{15}$$

For both methods, we have only included cells that produced a non-zero variance, i.e., we have excluded cells that remained in equilibrium from the calculation. The maximum standard deviation of all cells $s_{\max}$ is also computed. It is important to note that these are the relative variances in the angularly integrated intensity, not the radiation temperature. The radiation temperature has less noise.

Table **??** compares $\|s\|$ for IMC and HOLO with ECMC, for two different time-step sizes. All results in the table were generated with 12,000 histories per time step.

Table I: Comparison of sample standard deviations for the Marshak Wave problem for 200 x cells and 12,000 histories per time step. Simulation end time is $\mathrm{t} = 5$ sh.

	$\|s\|$		$s_{\max}$	
$\Delta t(sh)$	IMC	HOLO-ECMC	IMC	HOLO-ECMC
0.001	3.46%	0.36%	17.79%	7.70%
0.005	2.08%	0.78%	65.70%	29.84%

V.B. Two Material Problem

This problem consists of an optically thin (left) and an optically thick (right) material region, with constant opacities. The material properties are given in Table **??**. Initially the radiation and material energies are in

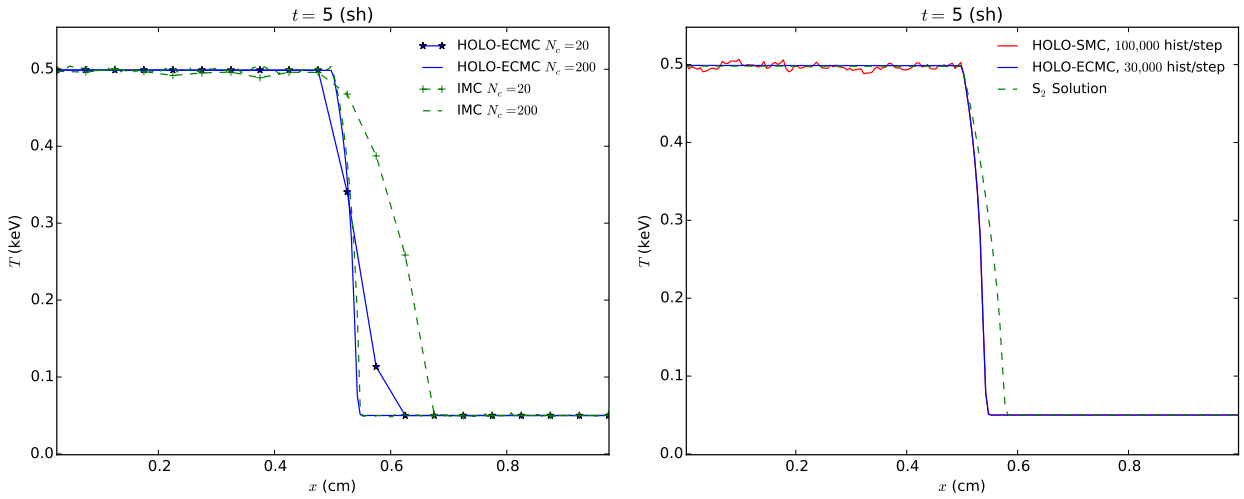

(a) Comparison of IMC and HOLO-ECMC.

(b) Comparison of SMC and ECMC HO solvers.

Figure 2: Comparison of radiation temperatures for two material problem.

equilibrium at a temperature of 0.05 keV. An isotropic incident intensity of 0.500 keV is applied at $x = 0$ at $t = 0$; the isotropic incident intensity on the right boundary is 0.05 keV. The simulation is ran for 5 sh. For all HOLO simulations, we have used 8 equal-sized mesh cells in μ.

Table II: Material properties for two material problem

	$x \in [0, 0.5)$ cm	$x \in [0.5, 1.0]$ cm
σ_a (cm$^-$1)	0.2	2000
ρ (g cm$^-$3)	0.01	10.0
c_v (jks/keV-g)	0.1	0.1

Fig. **??** compares the HOLO and IMC radiation temperatures at the end of the simulation. The IMC method used 10^5 histories per time step, where as the HOLO method used 3×10^4 histories per time step. The IMC and HOLO results show good agreement over the finer mesh. On the coarse mesh ($N_c = 20$), the HOLO method predicts the location of the wave-front more accurately than the IMC method.

Table III: Comparison of sample standard deviations for the two material problem for 200 x cells and 30,000 histories per time step. Simulation end time is t $= 2$ sh.

	$\|\|s\|\|$		$s_{\max}$	
$\Delta t(sh)$	IMC	HOLO-ECMC	IMC	HOLO-ECMC
0.001	7.45%	0.014%	19.90%	0.166 %
0.005	3.98%	0.022%	8.63%	0.159 %

V.C. Performance comparison of IMC and HOLO-ECMC

We have measured the total CPU time for simulations to provide a crude measure of the computational cost. These results provide a measure of how the methods compare for the two different problems and how

they scale with time step size and particle histories. Absolute comparisons in the computational cost of the two methods cannot be made because the methods are implemented in different code infrastructures. Additionally, the HOLO method fully resolves non-linearities at each time step, whereas IMC is using a single linearized step with lagged opacities.

Table **??** compares simulation CPU times, per history performed, for IMC and the HOLO method with ECMC. Results are given for different numbers of histories per time step, as well as a case with an increased time step size. The table also includes the number of LO iterations performed per LO solve, averaged over all time steps; there are two LO and one HO solve performed per time step. There is a slight increase in the number of newton iterations as the time step is increased. The HOLO method does not scale with the number of histories due to the fixed cost of the LO solver. The cost of the LO solver is more significant at 12,000 histories per time step where IMC takes less time, whereas at 10^5 histories the HOLO simulation takes less time. The gain in efficiency of the HOLO method over IMC would be significant if the large reduction in statistical error, for the same number of histories, is considered. Similar to the results in [**?**], as the time step size is increased to to 0.005 sh, the IMC method increases in cost (per time step) more than the HOLO method. The increase in the IMC simulation time with a larger time step is due to the increased amount of (expensive) effective scattering events.

Table IV: Total CPU times for the Marshak Wave problem for 200 x cells. Simulation end time is $\mathbf{t = 5}$ sh. For the HOLO solutions the average number of LO Newton iterations per LO solve are given.

Hists. per step	$\Delta t(sh)$	IMC	HOLO-ECMC	Iters./LO solve
10^5	0.001	5190 s	4003 s	3.8
1.2×10^4	0.001	635 s	692 s	4.1
1.2×10^4	0.005	303 s	179 s	6.2

Total CPU times for the two material problem are given in Table **??**. The end time for the simulations in this table was reduced to 2 sh. The observed behavior in the computational times is similar to those in the first problem. Because the opacities do not have a T^{-3} behavior in this problem, the cost of the effective scattering cross section in IMC is more apparent, resulting in longer simulation times. As the time step size is increased by a factor of 5, the average cost per time step for the simulation increases by a factor of ~ 3.4; for HOLO-ECMC the increase is only ~ 1.1.

Table V: Total CPU time required for the two material problem. Simulation end time is $\mathbf{t = 2}$ sh.

Hists. per step	$\Delta t(sh)$	IMC	HOLO-ECMC	Iters./LO Solve
10^5	0.001	3428 s	673 s	4.9
3×10^4	0.001	1036 s	397 s	5.0
3×10^4	0.005	699 s	86 s	7.6

V.D. Comparison of different HO Solvers

Fig. **??** compares results for different HO solvers. The HOLO algorithm with the ECMC HO solver (HOLO-ECMC) results are for running 3 batches of 10,000 histories, per time step. The solution for the HOLO method with a standard MC solver as the HO solver (HOLO-SMC) with standard source sampling uses 10^5 histories per time step. The HOLO-SMC solution demonstrates significant statistical noise. This

noise is introduced into the LO solver by bad statistics in computing the consistency terms. Also plotted is an S_2 solution obtained with consistency terms that are equivalent to S_2 and not performing the HO correction step in the algorithm. The S_2 solution results in an artificially fast wave front, as expected, demonstrating the necessity of HO correction in this problem.

To demonstrate the benefit of ECMC over RMC, we compare the variance for the two methods. We simulate RMC by performing a single batch in the ECMC solver. This is similar to the approach in [**?**], but with a slightly different source.

Table VI: Comparison of sample standard deviations for the Marshak Wave problem for 200 x cells and 12,000 histories per time step. Simulation end time is $\mathrm{t} = 5$ sh.

	$\|s\|$			$s_{\max}$		
$\Delta t(sh)$	HOLO-SMC	HOLO-RMC	HOLO-ECMC	HOLO-SMC	HOLO-RMC	HOLO-ECMC
0.001	3.05%	0.13%	0.36%	43.38%	2.26%	7.70 %
0.005	14.88%	0.25%	0.78%	63.48%	9.92%	29.84 %

Table VII: Comparison of sample standard deviations for the two material problem for 200 x cells and 12,000 histories per time step. Simulation end time is $\mathrm{t} = 2$ sh.

	$\|s\|$			$s_{\max}$		
$\Delta t(sh)$	HOLO-SMC	HOLO-RMC	HOLO-ECMC	HOLO-SMC	HOLO-RMC	HOLO-ECMC
0.001	3.01%	0.0095%	0.014%	7.92 %	0.559	0.166%
0.005	1.79%	0.0168%	0.022%	23.49%	0.493	0.159%

VI. Conclusions

VI.A. Summary

We have been able to produce solutions for Marshak wave test problems using a new HOLO method that is in agreement with IMC. Unlike IMC, our method requires no effective scattering events to be included in the MC simulation, limiting the total run time of the simulations. The LD spatial representation mitigates issues with teleportation error, similar to source tilting in the IMC algorithm. The LO solver resolves the non-linearities in the equations resulting in a fully implicit time discretization. The ECMC approach, with initial guesses based on the previous radiation intensity, results in efficient reduction of statistical error and allows for particles to be distributed to largely varying regions of the problem. The LO solver can accurately and efficiently resolve the solution in diffusive regions, while the HO transport solver provides the accuracy of a full transport treatment where necessary.

The primary difficulty to overcome in the HO solver is at the wave front. A strictly positive functional representation of the angular flux needs to be enforced for accurate solutions near the wave front. The representation needs to be implemented such that the spatial closure in the LO system is consistent with the HO representation for the solution. The ability to represent the solution accurately in rapidly varying regions of the problem will be key for generalization of this method to higher dimensions.

VI.B. Future Work

Future work will include comparisons of the HOLO method with IMC using a figure of merit to quantify the efficiency of the simulations when statistical noise is considered; the sensitivity of the method to mesh

sizes and time step sizes will be investigated more thoroughly. The loss of accuracy in optically thin regions due to the time discretization of the transport equation (which is required to form the residual in ECMC) will be analyzed. A formulazation of the ECMC method that allows for the trial space to be such that time-continous transport can be treated with Monte Carlo is currently being investigated; the additional sampling of the time variable will likely result in additional histories for problems where the time change is great over a time step. However, greater time accuracy is not of primary concern as this method isintended for use in regions of high absorption-reemission where the LO acceleration is critical.

Ultimately, we plan to extend this method to multiple spatial dimensions for the case of multigroup TRT equations. For TRT problems, it is important that the LO spatial discretization satisfies the equilibirium diffusion limit. To extend to higher dimensions, our LD FE representation may require the use of a higher-degree spatial representation for the LO system to achieve the diffusion limit. We will also investigate the possibility of using the HO MC solution to provide cell inflows such that the LO system correctly achieves the diffusion limit. Further asymptotic analysis on the method will be applied before implementation. It may be necessary to use a different LO system (e.g., the non-linear diffusion acceleration approach in [**?**]), if the S_2-like equations become too inefficient or difficult to implement in higher dimensions. Alternatively, a variable Eddington Tensor approach may provide more stability in rapidly variable regions of the problem while still being efficiently solved.

ACKNOWLEDGEMENTS

This research was performed using funding received from the DOE Office of Nuclear Energy's Nuclear Energy University Programs and under Los Alamos National Security, LLC, for the National Nuclear Security Administration of the U.S. Department of Energy under contract DE-AC52-06NA25396.

REFERENCES

[1] J. A. Fleck, Jr. and J. D. Cummings, Jr., "An Implicit Monte Carlo Scheme for Calculating Time and Frequency Dependent Nonlinear Radiation Transport," *J. Comput. Phys.*, **8**, 3, pp. 313–342 (Dec. 1971).

[2] N. Gentile, "Implicit Monte Carlo diffusion: An acceleration method for Monte Carlo time-dependent radiative transfer simulations," *Journal of Computational Physics*, **172**, 2, pp. 543–571 (2001).

[3] J. D. Densmore, K. G. Thompson, and T. J. Urbatsch, "A hybrid transport-diffusion Monte Carlo method for frequency-dependent radiative-transfer simulations," *Journal of Computational Physics*, **231**, 20, pp. 6924–6934 (2012).

[4] A. B. Wollaber, E. W. Larsen, and J. D. Densmore, "A Discrete Maximum Principle for the Implicit Monte Carlo Equations," *Nuclear Science and Engineering*, **173**, 3, pp. 259–275 (2013).

[5] J. Willert, C. Kelly, D. Knoll, and H. Park, "A Hybrid Approach to the Neutron Transport k-Eigenvalue Problem using NDA-based Algorithms," (2013), M&C.

[6] H. Park, J. Densmore, A. Wollaber, D. Knoll, and R. Ramenzahn, "Monte Carlo Solution Methods in a Moment-Based Scale-Bridging Algorithm For Thermal Radiative Transfer Problems," M&C (2013).

[7] J. Willert and H. Park, "Residual Monte Carlo High-order Solver for Moment-Based Accelerated Thermal Radiative Transfer Equations," *Journal of Computational Physics*, **276**, pp. 405 – 421 (2014).

[8] S. Bolding and J. Morel, "A High-Order Low-Order Algorithm with Exponentially-Convergent Monte Carlo for k-Eigenvalue problems," ANS Winter Meeting (2014).

[9] E. Wolters, *Hybrid Monte Carlo - Deterministic Neutron Transport Methods Using Nonlinear Functionals*, Ph.D. dissertation, Michigan (2011).

[10] J. Peterson, J. Morel, and J. Ragusa, "Exponentially Convergent Monte Carlo for the 1-D Transport Equation," M&C (2013).

[11] J. Morel, T. Wareing, and K. Smith, "Linear-Discontinuous Spatial Differencing Scheme for S_n Radiative Transfer Calculations," *Journal of Computational Physics*, **128**, pp. 445–462 (1996).

[12] J. Peterson, *Exponentially Convergent Monte Carlo for the 1-D Transport Equation*, Master's thesis, Texas A&M (2014).

[13] J. Shultis and W. Dunn, *Exploring Monte Carlo Methods*, Academic Press, Burlington, MA 01803 (2012).

[14] T. Urbatsch and T. Evans, "Milagro Version 2 An Implicit Monte Carlo Code for Thermal Radiative Transfer: Capabilities, Development, and Usage," Los Alamos National Laboratory Report LA-14195-MS (2006).

[15] M. S. McKinley, E. D. Brooks III, and A. Szoke, "Comparison of implicit and symbolic implicit Monte Carlo line transport with frequency weight vector extension," *Journal of Computational Physics*, **189**, 1, pp. 330–349 (2003).

[16] J. Edwards, J. E. Morel, and D. A. Knoll, "Nonlinear variants of the the TR/BDF2 method for thermal radiative diffusion," *Journal of Computational Physics*, **230**, 4, pp. 1198–1214 (2011).

A Implementation of ECMC Tallies

The ECMC solver uses a finite element representation in space and angle. On the interior of the cell with the i-th spatial index and j-th angular index, the linear representation is defined as

$$\tilde{I}(x,\mu) = I_{a,ij} + \frac{2}{h_x} I_{x,ij}\,(x - x_i) + \frac{2}{h_\mu} I_{\mu,ij}\,(\mu - \mu_j)\,, \quad x_{i-1/2} < x < x_{i+1/2}, \quad \mu_{j-1/2} \leq \mu \leq \mu_{j+1/2}$$

The spatial cell width is h_x, the angular width is h_μ, the center of the cell is (x_i, μ_j), and

$$I_{a,ij} = \frac{1}{h_x h_\mu} \iint\limits_{\mathcal{D}} I(x,\mu)\,\mathrm{d}x\mathrm{d}\mu \tag{16}$$

$$I_{x,ij} = \frac{6}{h_x h_\mu} \iint\limits_{\mathcal{D}} \left(\frac{x - x_i}{h_x}\right) I(x,\mu)\,\mathrm{d}x\mathrm{d}\mu \tag{17}$$

$$I_{\mu,ij} = \frac{6}{h_x h_\mu} \iint\limits_{\mathcal{D}} \left(\frac{\mu - \mu_j}{h_\mu}\right) I(x,\mu)\,\mathrm{d}x\mathrm{d}\mu, \tag{18}$$

where $\mathcal{D} : x_{i-1/2} \leq x \leq x_{i+1/2} \times \mu_{j-1/2} \leq \mu \leq \mu_{j+1/2}$. Standard upwinding in space is used to define $I(\mu)$ on incoming faces. This representation can directly be plugged into Eq. (11) and evaluated to produce the residual source in the ECMC HO transport problem.

During a MC batch, moments of the error are tallied. Moments of the error are defined analogously to Eq.'s (**??**)–(**??**). The tallies are evaluated by weighting the particle density with the appropriate basis function and integrating along the path. For the cell average, the n-th particle makes the contribution

$$\epsilon^n_{a,ij} = \frac{1}{h_x h_\mu} \int_{s^n} w^n(x,\mu)\mathrm{d}s \tag{19}$$

where s^n is the length of the n-th particle track in the cell and $w(x,\mu)$ is the weight of the error particle in the MC simulation. Substitution of the exponential attenuation of the weight produces the result

$$\epsilon^n_{a,ij} = \frac{w(x_0,\mu)}{\sigma_t h_x h_\mu} \left(1 - e^{-\sigma_t s^n}\right) \tag{20}$$

where $w(x_0,\mu)$ is the particle weight at the start of the path. The contribution of a particle track to ϵ_x is given by

$$\epsilon^n_{x,ij} = \frac{w(x_0,\mu)}{h_x^2 h_\mu \sigma_t} \left[x_0 - x_f e^{-\sigma_t s^n} + \left(\frac{\mu}{\sigma_t} - x_i\right)\left(1 - e^{-\sigma_t s^n}\right),\right] \tag{21}$$

where x_0 and x_f are the beginning and ending x coordinates of the n-th path. The contribution to the first moment in μ is

$$\epsilon^n_{\mu,ij} = \frac{w(x_0,\mu)}{h_\mu^2 h_x \sigma_t} \left(\mu - \mu_j\right)\left(1 - e^{-\sigma_t s^n}\right) \tag{22}$$

where the particle x-direction cosine μ does not change along the particle track because it is a pure-absorber simulation. The moments are simply the average contribution of all particles.

B HO fixup for radiation

NOT DONE???YET When the result of an ECMC batch produces a negative solution, the solution is modified to enforce a positive solution. Although the residual trial space allows for a positive result, allowing for the negative represnetation will cause errors in cells further downstream. After detecting a negativity at the end of a batch, the solution is modified such that the most negative part of the solution is positive, and the new solution preserves the calculated cell average $I_{a,ij}$, and the ratio of $I_{x,ij}$ to $I_{\mu,ij}$. first moment in μ to the first moment in x. Negative averages can occur occasionally do to statistics. In this case, the solution within that cell is set to the minimum temperature, i.e., the initial temperature of the simulation.